

UDSpace Institutional Repository
University of Delaware Open Access Articles

Ganesh, R., Sockalingam, S., (Gama) Haque, B., & Gillespie, J. (2016).
Dynamic effects of single fiber break in unidirectional glass fiber-reinforced
composites. *Journal Of Composite Materials*, 51(9), 1307-1320.
<http://dx.doi.org/10.1177/0021998316669218>

DOI: 10.1177/0021998316669218

This article is made available in accordance with the University of Delaware
Faculty Policy on Open Access ([4.2.15](#)) and the publisher's policy.

Dynamic effects of single fiber break in unidirectional glass fiber-reinforced composites

Raja Ganesh^{1,2*}, Subramani Sockalingam^{1,2}, Bazle Z. (Gama) Haque^{1,2} and John W. Gillespie, Jr. ^{1,2,3,4}

Abstract

In a unidirectional composite under static tensile loading, breaking of a fiber is shown to be a locally dynamic process which leads to stress concentrations in the interface, matrix and neighboring fibers that can propagate at high speed over long distances. To gain better understanding of this event, a fiber-level finite element model of a 2-dimensional array of S2-glass fibers embedded in an elastic epoxy matrix with interfacial cohesive traction law is developed. The brittle fiber fracture results in release of stored strain energy as a compressive stress wave that propagates along the length of the broken fiber at speeds approaching the axial wave-speed in the fiber (6 km/s). This wave induces an axial tensile wave with a dynamic tensile stress concentration in adjacent fibers that diminishes with distance. Moreover, dynamic interfacial failure is predicted where debonding initiates, propagates and arrests at longer distances than predicted by models that assume quasi-static fiber breakage. In the case of higher strength fibers breaks, unstable debond growth is predicted. A stability criterion to define the threshold fiber break strength is derived based on an energy balance between the release of fiber elastic energy and energy absorption associated with interfacial debonding. A contour map of peak dynamic stress concentrations is generated at various break stresses to quantify the zone-of-influence of dynamic failure. The dynamic results are shown to envelop a much larger volume of the microstructure than the quasi-static results. The implications of dynamic fiber fracture on damage evolution in the composite are discussed.

*Corresponding author

Phone no: 352-215-0463

Email: rganesh@udel.edu

¹Center for Composite Materials, University of Delaware, DE, USA

²Department of Mechanical Engineering, University of Delaware, DE, USA

³Department of Materials Science and Engineering, University of Delaware, DE, USA

⁴Department of Civil and Environmental Engineering, University of Delaware, DE, USA

Introduction

Glass fibers exhibit a statistical distribution of strength that depends on the size and spatial distribution of critical defects within the fiber. Under quasi-static axial tensile loading of a unidirectional glass fiber-reinforced polymer matrix composite, the stiff glass fibers are the major load carrying members. In the case of composites with matrices having higher strain to failure than the fibers, the fibers tend to fail first¹. Based on classical shear lag theory that considers pre-broken fibers under quasi-static loading (i.e. neglects dynamic effects), neighboring fibers experience a stress concentration at the break location. Stresses are transferred back into the broken fiber through shear in the interface and matrix to the original far-field stress state in a characteristic distance commonly referred to as the ineffective or recovery length. Depending on the magnitude of the stress concentrations and the stress recovery length, the initial breaks could trigger interfacial debonding and additional fiber breaks in the vicinity of the broken fiber, leading to formation of localized clusters of fiber breaks. It is hypothesized that once a critical cluster size is reached, the composite fails catastrophically²⁻⁴. These scenarios for predicting composite damage from a series of fiber breaks are based on classical shear lag mechanics associated with pre-broken fibers, where the dynamic aspects of brittle fiber failure are not considered.

The effect of a single pre-broken fiber in a composite has been studied extensively using analytical approaches based on the quasi-static shear lag analysis developed by Cox⁵. In this approach, it is assumed that the axial tensile load is carried entirely by the fibers and the matrix is capable of only carrying shear loads. The approach was applied to unidirectional composites by Hedgepeth⁶ when he studied the stress concentrations due to a pre-broken fiber within an infinite 2-dimensional array of fibers. This was further extended to infinite hexagonal and square arrays of fibers by Hedgepeth and van Dyke⁷. Beyerlein and Phoenix⁸ developed a technique called quadratic influence superposition to improve the predictions of the 2D shear lag model by considering local matrix yielding. Landis and McKeening enhanced the shear lag approach to take into account the effect of interface sliding⁹ and plasticity in a ductile matrix¹⁰. Beyerlein and Landis¹¹ developed a shear lag model which considers the axial load carrying capability of the matrix. Okabe et al.¹² developed a 3D shear lag model with a square packing of fibers where the matrix is modeled as shear springs connecting neighboring fibers. All of these analytical studies consider the mechanics of a pre-broken fiber and neglect dynamic effects associated with brittle fiber failure in the composite. However, they provide useful baseline results to compare with the results presented in this paper in order to understand the importance of dynamic fiber failure.

With the increase in computational capabilities over the years, Finite Element (FE) Modeling has become an excellent alternative for studying stress redistributions at the fiber length-scale while eliminating many of the inherent assumptions in the various shear lag models¹. Nedele and Wisnom^{13,14} used a 3D FE model to study the stress concentration factors in the vicinity of a single pre-broken fiber in a hexagonally packed unidirectional composite. They assumed that the matrix remains entirely elastic and that a perfect bonding exists between the fiber and matrix materials. Goda et al.¹⁵ used a

simplified FE model where the interface was modeled using discrete spring elements in order to study the effect of interface shear strength on the macroscopic strength of a unidirectional composite. van Den Heuvel et al.¹⁶ used a 3D FE model where they included the effects of matrix plasticity. They studied the effects of interface failure by explicitly introducing partial debonding of the interface along the broken fiber prior to loading but did not study debond growth. These numerical studies on quasi-static loading of pre-broken fibers show that interface debonding is an important failure mechanism to include in our study on dynamic effects of fiber breaks in composites.

Even under static applied loads, the breaking of glass fibers is a locally dynamic event due to the brittle nature of their failure. Swolfs et. al.¹⁷ used Synchrotron radiation computed tomography for in-situ observation of tensile failure in unidirectional composites. They loaded the composite specimen to different percentages of its nominal failure load and observed that co-planar clusters of fiber breaks formed within a single strain increment. They simulated the experiment using a strength model^{18,19} where the stress concentration profiles due to a fiber break were determined using a quasi-static FE model with a pre-broken fiber. The model predicted a more gradual progressive development of clusters as opposed to the sudden formation of co-planar clusters observed in the experiment. The authors pointed out that one of the main reasons for this discrepancy could be the fact that the state-of-the-art models ignore the dynamic effects of fiber failure.

However, very little work has been done in terms of studying the dynamic effects of a fiber break. Hedgepeth⁶ had modeled the dynamic stress concentrations at the plane of the fiber break in a fiber next to a broken fiber using his simplified shear lag solution. He illustrated that the stress concentration factor exhibits an oscillation that decays to the steady-state (static) value in a few cycles. Ji, Liu and Chou²⁰ modeled the dynamic stress concentration factors not just at the plane of the fiber break, but also along the entire length of a fiber next to a broken fiber using the classical shear lag approach. Their results indicate that the dynamic effects are significant only for a very short time scale of the order of $10\sqrt{(m_f d / G_m)}$, where m_f , d and G_m represent the mass-per-unit-area of the fiber, the fiber diameter, and the shear stiffness of the matrix, respectively. For typical Glass-epoxy composites such as the one considered in this paper, this time scale is in the order of 50 nanoseconds. Current advanced high-speed sensing capabilities using Phase Contrast Imaging (PCI) in an X-ray synchrotron can only achieve a temporal resolution of 100 nanoseconds²¹. Thus, it is extremely challenging to experimentally characterize dynamic effects of fiber breaks within a composite in real time. Therefore, numerical modeling becomes an essential tool to study and quantify these effects while eliminating many of the assumptions in shear lag theory.

In this paper, the problem of a single fiber break and the associated stress redistribution is studied using an FE model of a 2D-planar array of fibers interspersed with matrix regions. In reality, fibers have a circular cross-section and they are packed randomly in the cross-section of the composite. However, since the focus of the present paper is on elucidating the mechanisms associated with dynamic fiber break, we are using a 2D-planar array of fibers in our models. This also allows us to compare our results with the analytical shear lag solution. The problem is first studied using a quasi-static model

with a pre-broken fiber which does not consider any dynamic effects. Next, the same problem is simulated as a transient dynamic problem where the inertial effects of the fiber break and the associated wave propagation mechanisms are captured.

The remainder of the paper is organized into 3 major sections: 1) ‘Physical problem formulation’ which briefly describes the physics of the dynamic problem along with the material properties of the fiber and the matrix. 2) The subsequent section describes the details of the FE models used. These are 3D FE models with unit thickness and with the through thickness Poisson’s ratios set to zero. The fiber and matrix are modeled as elastic materials and the interfacial debonding mechanism is captured using a traction law that is derived from micro-droplet experiments on the same fiber-matrix system. This section ends with a numerical validation of the FE model. This is achieved by incorporating all the assumptions used in the classical dynamic shear lag solution into a simplified version of our FE model and then comparing the two solutions. 3) The ‘Results and Discussion’ section describes the key results of this work and their implications.

Physical problem formulation

Let $\boldsymbol{\sigma}$ denote the Cauchy stress tensor at a material point in the composite. From conservation of linear momentum, after neglecting body forces, we get the following governing equation (Eq. 1) which has to be satisfied at every material point:

$$\nabla \cdot \boldsymbol{\sigma} = \rho \mathbf{a} \quad (1)$$

where, ρ denotes the mass density and \mathbf{a} denotes the acceleration vector at the same material point. The ‘ $\rho \mathbf{a}$ ’ term on the right hand side is the inertial term which incorporates the effects of dynamic fiber break. If the dynamic effects of fiber failure are ignored, then the problem can be formulated as a quasi-static problem with a pre-broken fiber and the governing equation reduces to the static equilibrium equation:

$$\nabla \cdot \boldsymbol{\sigma} = \mathbf{0} \quad (2)$$

Material properties

In the present study, an S2-glass/Epoxy composite is considered. The fiber diameter (d) is chosen to be 10 microns, which is the typical diameter of an S-2 glass fiber²². The fiber volume fraction is considered to be 50%, which corresponds to an inter-fiber distance of 10 microns, since this is a 2D planar arrangement of fibers. Both the fiber and matrix materials are assumed to be linear-elastic. The elastic material properties used in this model are obtained from Sockalingam et. al.²³, and are listed in Table I. The density of S2-glass fibers is obtained from Song et. al.²⁴.

Table I. Baseline properties of fiber and matrix

Property	S-glass Fiber	Epoxy DER353
Young's Modulus (GPa)	90.0	3.2
Poisson's ratio	0.17	0.36
Density (gm/cc)	2.45	1.5

S2-glass fibers exhibit a statistical strength distribution which is typically described using a Weibull probability density function in the following form ²⁵:

$$P(\sigma, L) = 1 - \exp \left[- \frac{L}{L_0} \left(\frac{\sigma}{A} \right)^\beta \right] \quad (3)$$

where, $P(\sigma, L)$ is the cumulative probability of failure of a fiber of gage length L at a stress level of σ . A and β are experimentally-determined constants called the scale and shape parameters, respectively, and L_0 is the reference gage length at which these parameters are determined. The Weibull probability distribution for 5 mm gage length ($L=5$ mm) epoxy-compatible S-glass fibers obtained from Gurvich et. al. ²⁶ is considered in this paper. The Weibull scale and shape parameters are $A = 2644.8$ MPa and $\beta = 4.52$ for a reference gage length (L_0) of 25.4 mm. The distribution is shown in Fig. 1. The average of the distribution is 3.5 GPa for a gage length of 5 mm.

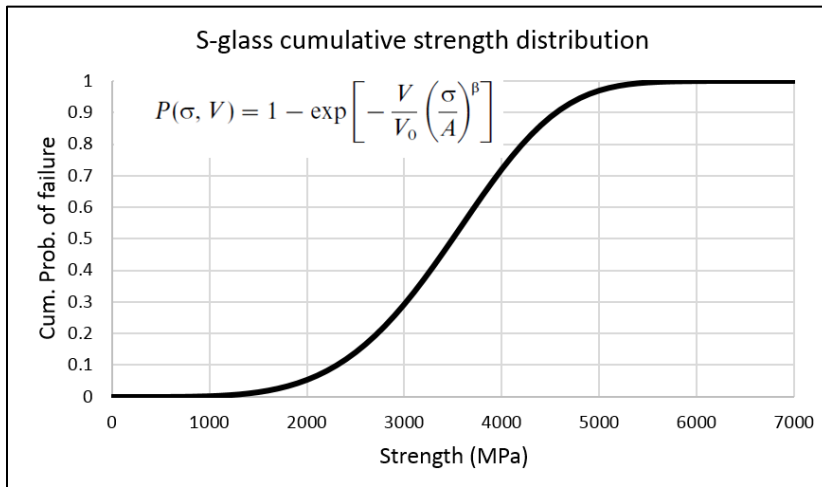


Fig 1: Weibull probability of failure distribution for 5-mm gage length S-glass fibers ²⁶

Dynamic progression of events after fiber fracture

Fig. 2 summarizes the dynamic progression of events immediately following a fiber break. We assume that the central fiber (Fiber 0) breaks at the $x=0$ plane at a break strength of σ_b . Just before the fiber break, the composite is in a state of iso-strain in the axial direction, i.e., $\epsilon_x = \epsilon_b = \sigma_b/E_f$ everywhere in the composite. As soon as the fiber breaks (Fig. 2a), the fiber free ends begin to spring back initiating a compressive axial stress wave along the length of the broken fiber (Fig. 2b). Due to the energy released from the fiber break, debonding initiates in the interface surrounding the broken fiber (Fig. 2c). The axial deformation associated with the unloading of the broken fiber induces a shear wave in the matrix. The shear wave induces axial stress in the adjacent fiber (Fiber 1). This axial stress is compressive downstream of the shear wave front and tensile behind the shear wave front. These axial stress waves, when superposed with the applied tensile stress, lead to the dynamic lowering and increasing of the tensile stresses in the adjacent fiber that propagate and decay in magnitude over long distances. The increase in axial stress due to the tensile part of the stress wave causes dynamic stress concentrations in the adjacent fiber.

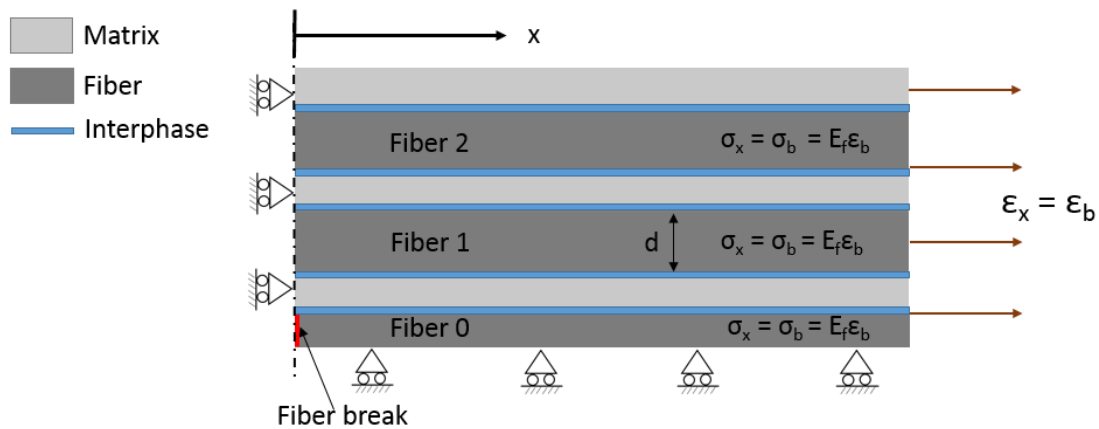


Fig 2a: Time, $t = 0$; Dynamic fiber fracture

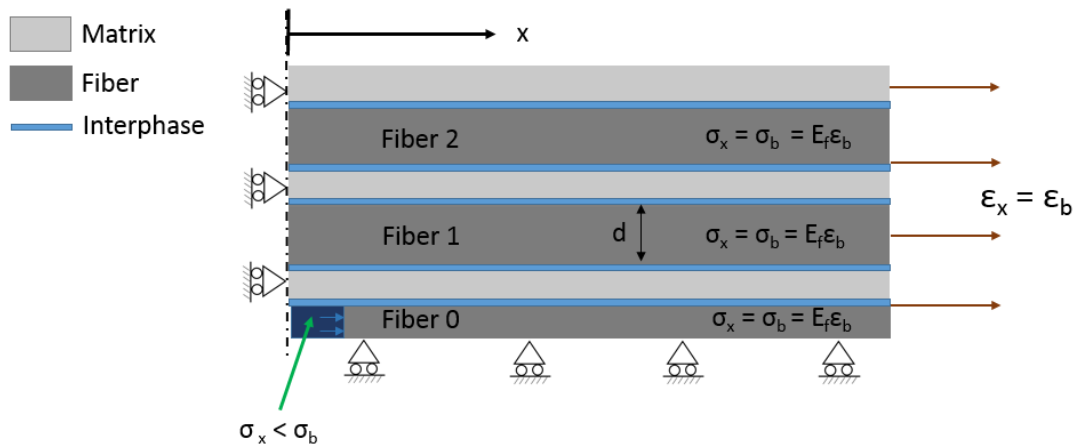


Fig 2b: Time, $t_1 > 0$; Compressive stress wave initiates in broken fiber

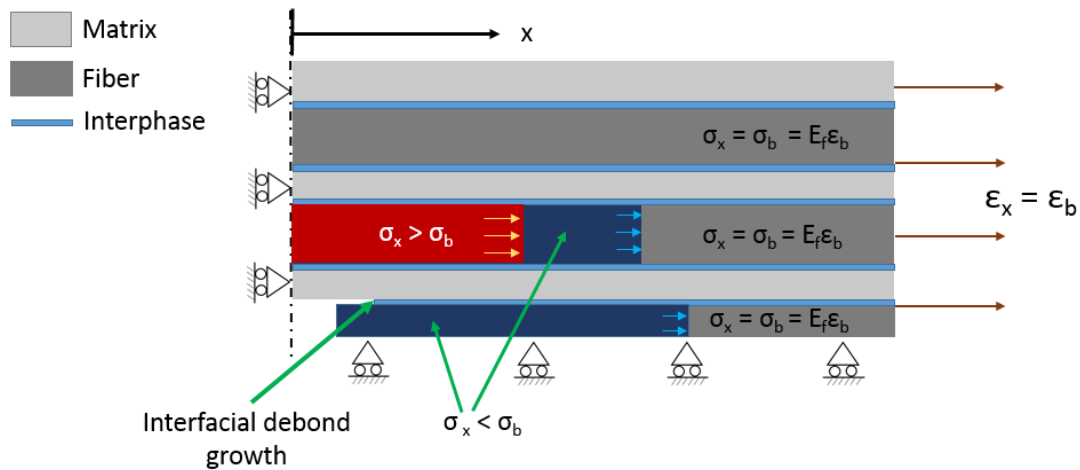


Fig 2c: Time, $t_2 > t_1$; Stress concentration propagates as a tensile stress wave in the neighboring fibers. Interfacial debonding propagates along the boundaries of the broken fiber

The longitudinal wave-speed in S-2 glass fiber is $c_f = \sqrt{\frac{E_f}{\rho_f}} = 6.06 \text{ km/s}$. A characteristic time, t_c , is defined as the time taken by the stress wave to propagate through a distance of one fiber diameter. This characteristic time is used to normalize the time dependent results presented below. For a fiber diameter of 10 microns, this translates to a characteristic time, $t_c = \frac{d}{c_f} = 1.65 \text{ ns}$. Since the Weibull strength distribution in the fibers is typically determined from tests where the stress is constant over the cross-section, the Stress Concentration Factor (SCF) in any fiber cross-section is

defined as the ratio of the average axial stress ($\sigma_{x,avg}$) in that cross-section over the applied nominal stress in the fiber, σ_{app} . This is analogous to the definition of SCF used in ²⁷. It should be noted that in reality, the strength distribution of the fibers is expected to be governed by critical surface defects on the fiber. In the present problem, $\sigma_{app} = \sigma_b$ for all the fibers. In a given fiber, the SCF in a cross-section at the location x' is defined as:

$$SCF (x = x') = \frac{\sigma_{x,avg}(x = x')}{\sigma_{app}} \quad (4)$$

Finite Element Model

A 3-dimensional finite element model with one element through the thickness is constructed using the commercial FE code ABAQUS. A 3D formulation with unit thickness is used instead of using 2D plane stress elements, since the surface-based cohesive contact can be used only between 3D solid elements in ABAQUS. The fiber and matrix are modeled using first order 8-noded hexahedral elements with full integration. The Poisson's ratios along the thickness directions (ν_{xz} and ν_{yz}) are set to zero in all the elements in order to eliminate the creation of stresses in the through thickness direction due to the mismatch in Poisson's ratio between the fiber and the matrix. The central fiber is allowed to break at a specified stress by releasing the tractions in the cross-section at $x=0$. The interface between the central fiber (the fiber that will break) and the matrix is modeled using surface-based cohesive contact. A uniform element size of 1.25 μm is employed in the entire model. The absolute difference in the peak dynamic SCF between models with element size of 2.5 μm and 1.25 μm is only 1.5% (Peak dynamic SCF is 1.352 for element size of 2.5 μm and 1.367 for element size of 1.25 μm). Also, the absolute difference in the static SCF is only 2.1 % (1.199 for 2.5 μm and 1.225 for 1.25 μm). The length of the model is chosen to be 2000 μm and the model contains 10 fibers on one side of the broken fiber with matrix regions interspersed between them. These overall dimensions are sufficient enough to ensure that the stress waves do not reach any of the boundaries throughout the simulation. Fig. 3 shows the FE model along with the boundary conditions used.

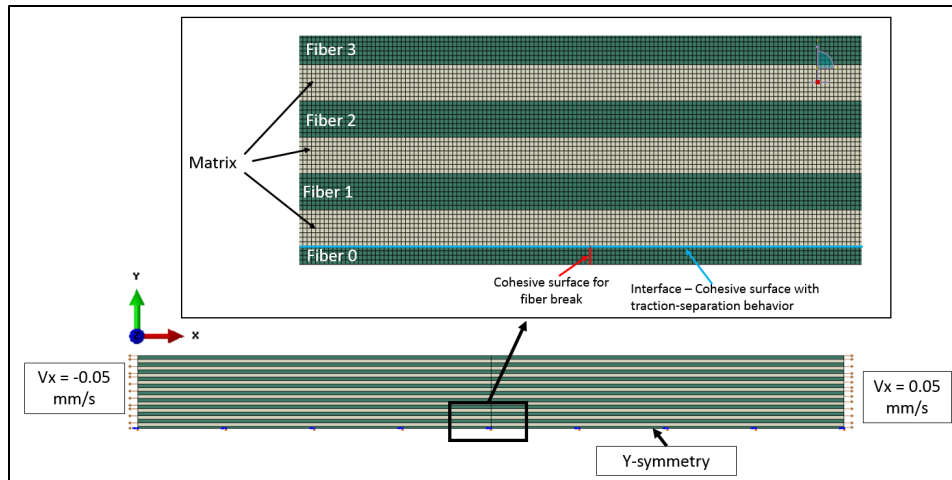


Fig. 3: Fiber-level FE model

Traction law for fiber-matrix interface

The fiber-matrix interface is modeled using surface-based cohesive contact formulation in ABAQUS. A mixed-mode bilinear traction-separation law is used to define the constitutive behavior of the interface. Damage initiation is modeled using a mixed-mode quadratic criterion and post-damage softening using a power law. The traction law for Mode I (opening mode) is assumed to be the same as for Mode II (shear mode). The parameters of the traction law are chosen from the FE modeling of the microdroplet experiment on the same fiber-matrix system²³. A peak traction of 120 MPa and a Mode II critical energy release rate (G_{IIc}) of 160 J/m² is used for the interface. For details on this interface model, the reader is referred to Sockalingam et. al.²³.

Modeling the fiber break

The fiber break is also modeled using a zero-thickness cohesive surface with a bilinear traction-separation behavior as shown in Fig. 4. The Stiffness of the cohesive surface is chosen to be a sufficiently high value (9×10^9 GPa/m) in order to maintain continuity of displacements across the cohesive surface until the fiber breaks. Mode I fracture of the cohesive surface is initiated at a specified value of average fiber axial stress using a maximum stress criterion. The critical strain energy release rate in the fiber, G_{Ic} is 10 J/m² and is typical of the surface energy in silica-based glass²⁸. Due to the low value of G_{Ic} , the fiber break takes place within a single time-step ($< 0.1 \cdot t_c$) in the model. i.e., the fiber break occurs instantaneously across the entire cross section which is equivalent to the assumption used in previous analytical dynamic shear lag theory solutions^{7,20}. This allows us to validate the numerical model with the analytic solution before incorporating dynamic debonding effects.

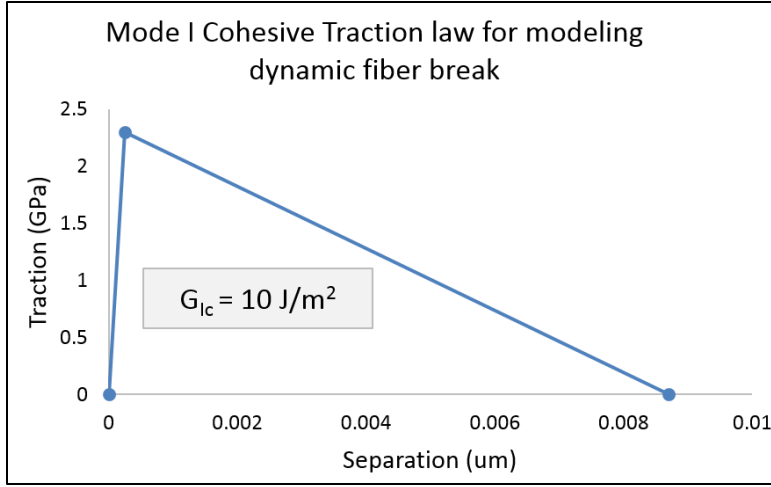


Fig. 4 : Cohesive traction law used for modeling dynamic fiber break at a break strength of 2.3 GPa

Model validation with classical dynamic shear lag solution

The classical shear lag solution for dynamic stress concentration factors obtained by Hedgepeth⁶ and later by Ji, Liu and Chou²⁰ employed the following assumptions:

- Fiber and Matrix are linear elastic
- Fibers carry only axial load
- Matrix carries only shear
- There is perfect bonding between the fiber and the matrix
- Mass is concentrated at the fiber centers
- Poisson's effects are ignored
- Strain rate effects are ignored

Based on these assumptions, considering a 2-dimensional arrangement of fibers with unit thickness, the dynamic equilibrium equation in the nth fiber is:

$$E_f d \left(\frac{\partial^2 u_n}{\partial x^2} \right) + \frac{G_m}{h} (u_{n+1} + u_{n-1} - 2u_n) = m_f \left(\frac{\partial^2 u_n}{\partial t^2} \right) \quad (5)$$

$(n = -\infty, \dots, -2, -1, 0, 1, 2, \dots, \infty)$

where, E_f is the young's modulus of the fiber,

m_f is the mass per unit area of the fiber,

G_m is the shear modulus of the matrix,

d is the fiber diameter

h is the width of the matrix region between two neighboring fibers

$u_n(x, t)$ is the displacement field in the nth fiber.

The axial tensile stress on the nth fiber is given by:

$$\sigma_n = E_f \left(\frac{\partial u_n}{\partial x} \right) \quad (6)$$

Assuming that the 0th fiber breaks at time, $t=0$, the following initial and boundary conditions are applied.

Initial conditions: $\sigma_n(x, 0) = \sigma_b$ (for all n) (7)

$$\frac{\partial u_n}{\partial t}(x, 0) = 0 \text{ (for all } n) \quad (8)$$

Boundary conditions: $\sigma_0(0, t) = 0$ (9)

$$u_n(0, t) = 0 \text{ (for } n \neq 0) \quad (10)$$

$$\sigma_n(\pm\infty, t) = \sigma_b \text{ (for all } n) \quad (11)$$

In order to match the assumptions used in the classical shear lag solution, the matrix is modeled as an orthotropic material with its axial stiffness reduced from 3.2 GPa to 100 MPa. This translates to the matrix carrying only 0.1% of the applied axial load.

The in-plane shear modulus of the matrix was unchanged from that of the baseline matrix material (1.18 GPa). The density of the matrix is also made negligible as opposed to the density of the fiber ($\rho_m \sim 0.001 * \rho_f$). The fiber-matrix interface is not allowed to debond in order to simulate perfect fiber-matrix adhesion. All Poisson's ratios in both the fiber and the matrix are set to zero. Fig. 5 shows the evolution of stress concentration factor with time in the neighboring fiber (Fiber 1) at $x=0$. The solution obtained from the FE element model closely matches the result obtained using Hedgepeth's solution proving the mesh and time resolution for our numerical model is sufficient to study the mechanisms of dynamic fracture. The solution shows that the dynamic SCF is 1.53 and drops to the static value of 1.33 in 2 cycles over 80 characteristic times.

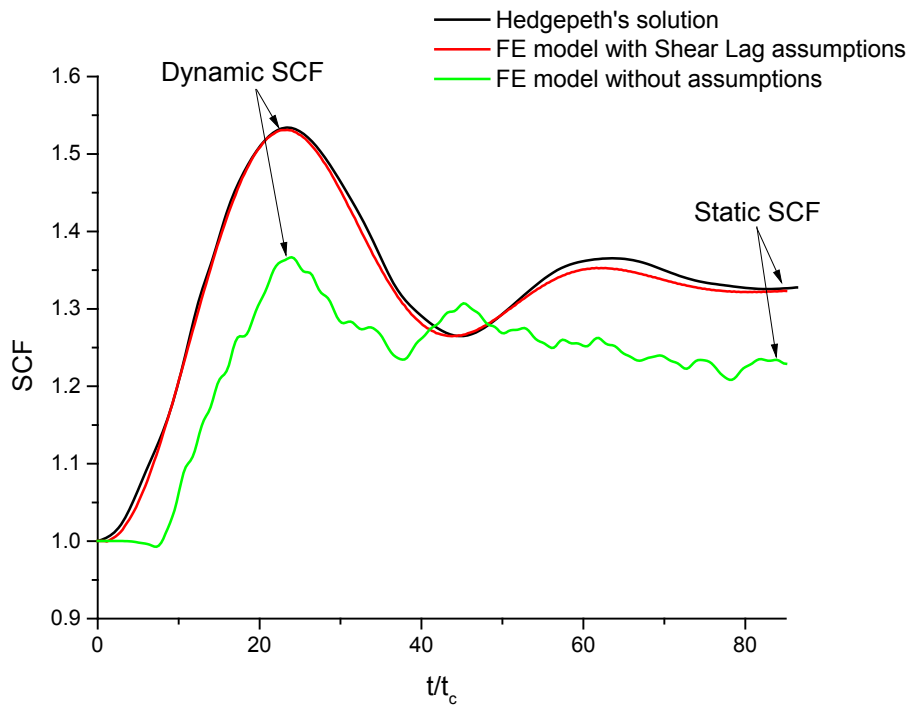


Fig. 5: Comparison of FE model results with Classical shear lag theory (SCF vs time in Fiber 1 at $x=0$). Data points in FE models collected at intervals of $\sim 0.3 * t_c$

Results and discussion

If the shear lag assumptions are relaxed in our numerical model, it can be seen that the shear lag solution over-predicts both the dynamic SCF (1.53 vs 1.36) as well as the static SCF (1.33 vs 1.23) as shown in Fig. 5. This can be attributed to the fact that the classical shear lag solution ignores the axial load carrying capability of the matrix. The

reduction in static SCF due to the consideration of the axial load carrying capacity of the matrix was also reported by Ochiai et. al. ²⁹ using a modified shear lag solution. The FE model also correctly predicts a time delay (approximately 7 characteristic times in Fig. 5) to load the adjacent fiber that is associated with shear wave propagation across the 10 micron matrix region. The shear wavespeed in the matrix is given by, $c_{m_sh} = \sqrt{\frac{G_m}{\rho_m}} = 0.886 \text{ km/s}$. Based on this value, the shear wave will propagate across the 10 micron matrix region in approximately 7 characteristic times.

In the baseline model, the first fiber break is assumed to occur at a fiber stress level of 2.3 GPa, which corresponds to a probability of failure of 10% (see Fig. 1). First, the problem is modeled as a static problem, where it is assumed that the fiber is already broken at the $x=0$ plane. The composite is then externally loaded to a strain level corresponding to a uniform fiber stress of 2.3 GPa. Next, the same problem is solved as a dynamic problem, using the Abaqus explicit solver. As soon as fiber failure occurs, an axial compressive stress wave is launched in the broken fiber. This stress wave propagates at a wave speed of 5.95 km/s. This is close to the theoretical 1-dimensional axial wave speed (c_f) of 6.06 km/s in the fiber material.

This compressive stress wave that travels along the broken fiber (Fiber 0 in Fig. 2c) leads to dynamic debonding of the interface around the broken fiber. The evolution of debond length with time is shown in Fig. 6. The debonding initiates at $10*t_c$ and propagates to a length of 6 fiber diameters before arresting at $40*t_c$. The velocity of the debond front exhibits a maximum speed of 1.06 km/s at t/t_c of 25. Since this is much slower than the axial wave speed in the fiber material, the debond front lags behind the compressive stress wave front as shown in Fig. 2c.

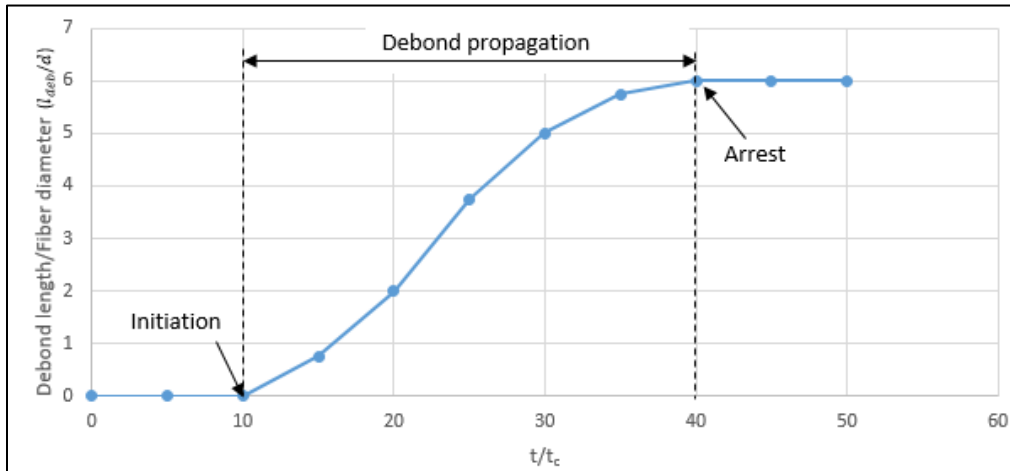


Fig 6: Interfacial Debond length vs time for the broken fiber (Fiber 0)

Fig. 7 shows a plot of the stress profile and interfacial damage parameter associated with Fiber 0 at time, $t = 100 * t_c$. The damage parameter is a scalar variable which linearly varies from 0 (No separation) to 1 (complete separation). Interfacial debond length (l_{deb}) is calculated as the length over which the damage variable is greater than 0.99. The length of the cohesive zone where energy absorption occurs is approximately 7 fiber diameters long at each crack tip. The stress profile obtained from the Quasi-static simulation is also included for comparison (no debonding is predicted in this case). The ineffective length, l_{ineff} (length over which Fiber 0 recovers 90 % of its load carrying capability) increases by one debond length (l_{deb}) in the dynamic solution ($l_{ineff_dyn} \sim 42 * d$) compared to the quasi-static solution ($l_{ineff_sta} \sim 36 * d$). More details on interfacial debonding and its implications will be presented in the following sections.

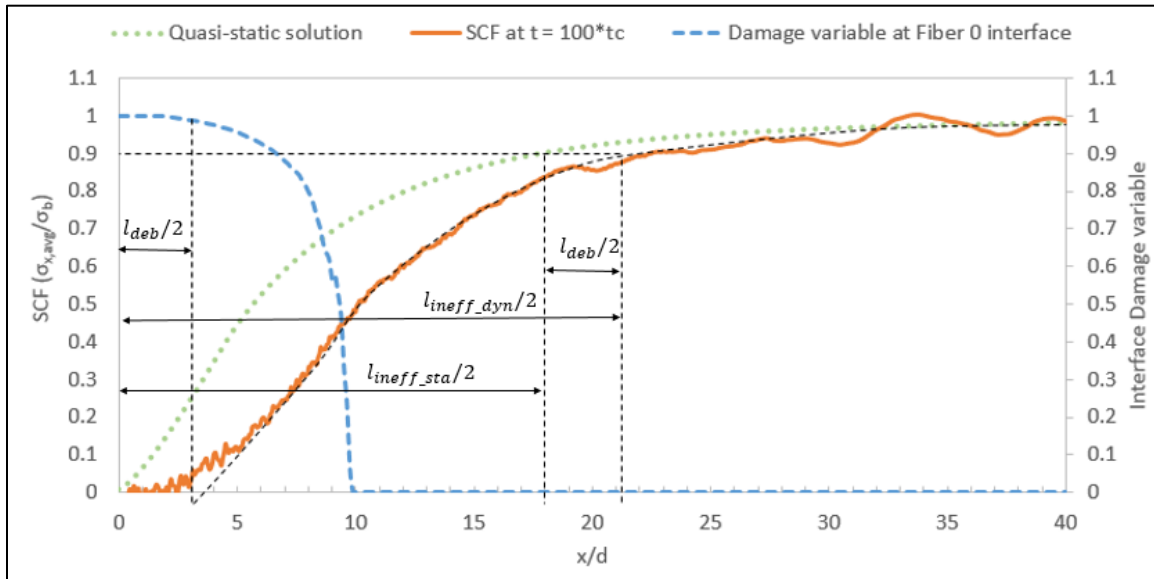


Fig 7: Stress profile at time, $t = 100 * t_c$ in broken fiber (Fiber 0). Figure also shows the profile of the interfacial damage variable in Fiber 0.

In the neighboring fiber, a stress concentration is induced and this propagates along its length as a tensile stress wave with a speed of 5.87 km/s, which is once again approaching c_f . Fig. 8 shows the evolution of stresses in the neighboring fiber vs. time at various distances from the fiber break. The smaller wavelength oscillations in the curves can be attributed to 1) secondary waves that are created due to the mismatch in Poisson's ratio between the fiber and the matrix, and 2) the reflections of stress-waves from the lateral boundaries of the fibers (at the fiber-matrix interfaces) due to impedance mismatch between the two materials. The results for $x/d=0$ are identical to the results in Fig. 5. At $x/d=10$, one can see the pattern of the dynamic response present at all x/d locations shown schematically in Fig. 2c. The delay in arrival time of dynamic SCF is evident. The amplitude first decreases with the arrival of the compressive wave and then increases

to its maximum tensile level before decaying to the static solution at large time. One also observes the decay in the peak SCF with increasing distance from the fiber break plane ($x/d=0$).

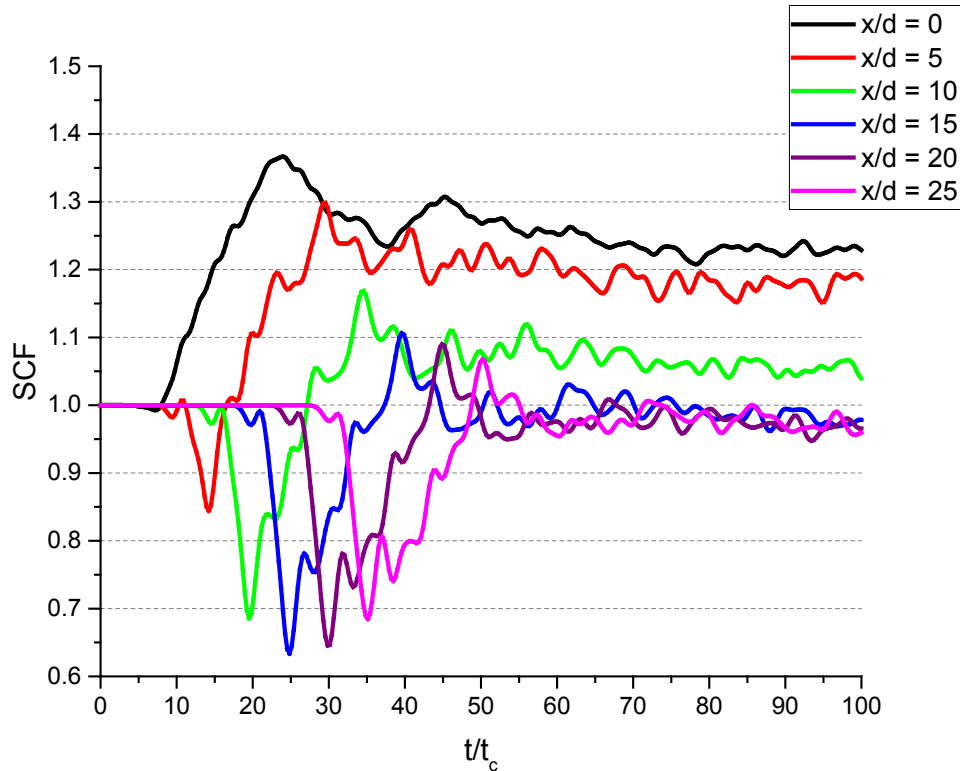


Fig 8: Time evolution of SCF at various cross-sections in the neighboring fiber (Fiber 1). Data points collected at intervals of $\sim 0.3 * t_c$

Fig. 9 shows the SCF profile in the neighboring fiber at $t = 100 * t_c$ which corresponds to the time at which the stress wave in the broken fiber (Fiber 0) reaches the boundary of the model at $x/d=100$. In this case, the wave in Fiber 1 has some time lag and has not reached the boundary. The quasi-static solution is included for comparison purposes. Recall that the quasi-static solution does not have any interfacial debonding and exhibits the maximum SCF at the fiber break cross-section and has an overload length of approximately 20 fiber diameters. Also shown in Fig 8 is the envelope of maximum dynamic SCF along the length of the fiber during this time. The fiber is subjected to significantly higher dynamic SCFs than the quasi-static model predictions that extend over a distance of 60 fiber diameters on either side of the break plane ($x/d = 0$). The results at $100 * t_c$ show evidence of interface debonding. At $x/d=0$ the SCF has decreased compared to the maximum SCF that occurs at $25 * t_c$ prior to the arrest of interfacial debonding. A 38 % increase in the overload length (length over which SCF drops to 1) is predicted. This is due to the interfacial cohesive traction law²³ that undergoes progressive softening prior to separation.

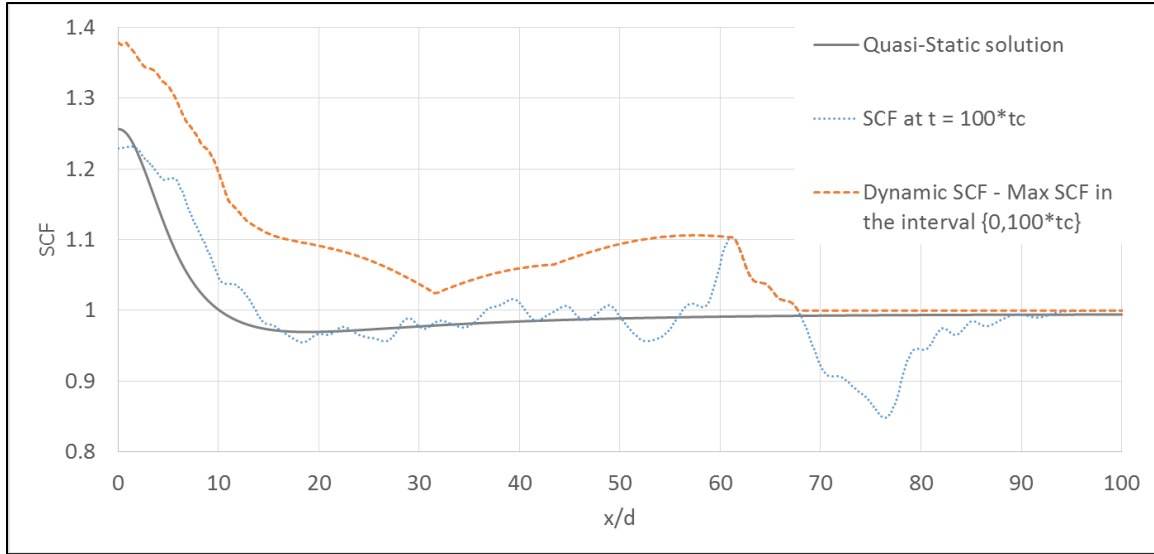
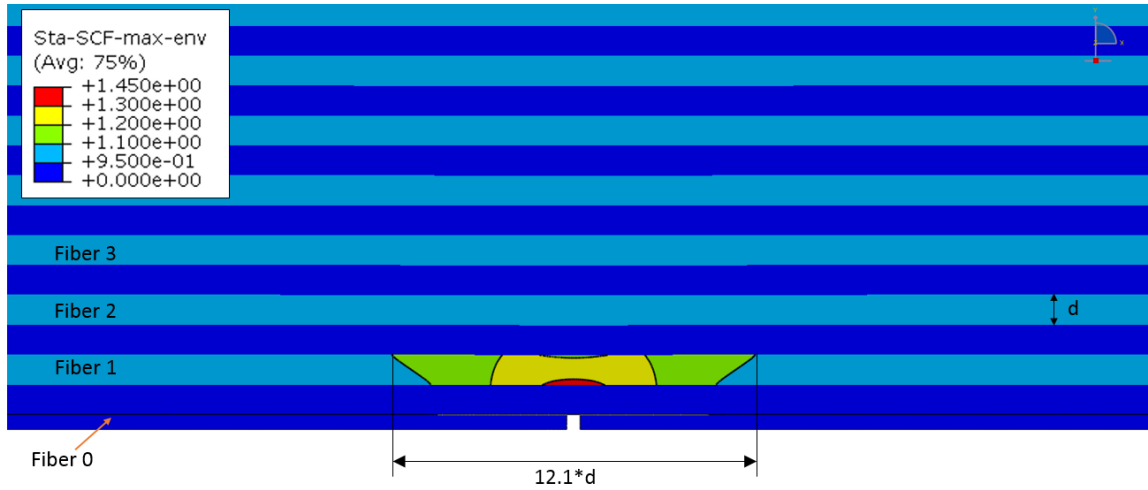
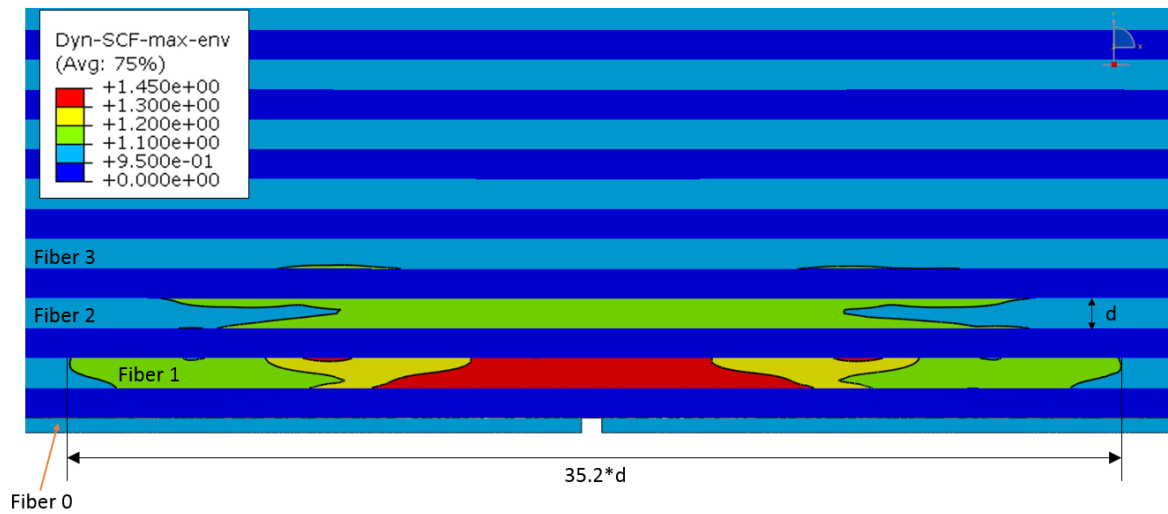


Fig 9: SCF profiles in neighboring fiber (break strength = 2.3 GPa)

Apart from causing an increase in the peak SCF at $x=0$, the dynamic effects of the fiber break also cause an appreciable increase in the area of influence of the fiber break. In order to quantify this effect, we define a zone-of-influence of the fiber break as the area over which the dynamic SCF in the neighboring fibers increases the probability of failure of additional fiber breaks. Recall that in this baseline simulation our fiber breaks at 2.3 GPa that corresponds to a 10% probability of failure. The zone of influence can be constructed based on stress level and associated probability of failure. For example, consider an SCF of 1.1 (i.e 2.53 GPa that corresponds to 15% probability of failure). As shown in Fig. 10, the zone of influence is about 5.3 times higher in area if we take the dynamic stress concentrations into account. The increase in the zone-of-influence is more pronounced along the fiber direction due to the higher wave-speeds along the fiber direction as opposed to the transverse direction since the shear wave-speed in the matrix (0.886 km/s) is much smaller compared to the axial wave-speed in the stiff glass fibers (6.06 km/s).



(a)



(b)

Fig. 10 : Comparison of Zone-of-influence of fiber break based on SCF of 1.1 (15% probability of failure) (a) Quasi-static simulation (b) Dynamic model with inertial effects
Note that only the SCFs in the fibers are shown in the images.

Interfacial Debonding

Depending on the Mode II fracture properties of the interface, there exists a critical level of break strength, σ_b , beyond which a fiber break will lead to unstable debonding of the interface. This critical break strength can be calculated using a simple energy balance formulation since both the fiber and matrix are assumed to be linear elastic. If the elastic strain energy stored in the fiber per unit length of fiber before the break is greater than the fracture energy required to debond the entire interface around the fiber per unit fiber length, then unstable debonding occurs.

The strain energy stored in the fiber per unit fiber length before the break,

$$U_f = \frac{\sigma_b^2}{2E_f} * (d * b) \quad (12)$$

Energy required to debond unit length of the interface on both sides of the fiber,

$$U_{deb} = G_{IIc} * (2 * b) \quad (13)$$

where, σ_b is the fiber break strength,

E_f is the Young's modulus of the fiber.

G_{IIc} is the Mode II critical energy release rate of the interface

d is the fiber diameter

b is the width of the 2D composite

Unstable debonding occurs when $U_f > U_{deb}$. Therefore, the critical strength at which a fiber break will lead to unstable debonding is the strength at which $U_f = U_{deb}$. i.e., when:

$$\sigma_b = \sqrt{\frac{4G_{IIc}E_f}{d}} \quad (14)$$

For the current fiber-matrix-interface combination under consideration, if the fiber break occurs at any load above 2.4 GPa, then it will lead to unstable debonding of the interface. Recall, the baseline simulation results presented above were generated for a breaking strength of 2.3 GPa that exhibited initiation, propagation and arrest of the interface debonding. For fiber strengths above 2.4 GPa, in the absence of friction between the debonded fiber and the matrix, arrest of the interface debonding is not predicted. Considering the zone of influence based on SCF of 1.1 (2.53 GPa) given in Fig. 10b, additional fiber breaks would trigger unstable growth within this region. This unstable debonding is consistent with the axial splitting failure mode that is experimentally observed in unidirectional composites under tensile loading³⁰. It is noteworthy that for this particular composite, the threshold for unstable debonding is well below the mean of the fiber strength distribution for the chosen gage length of 5 mm (i.e 3.5 GPa) implying that the translation of inherent fiber strength into the composite is governed by the dynamic failure and energy absorption of the interface debonding mechanism.

Dynamic debonding versus fiber break load

In the stable debond regime ($\sigma_b < 2.4 \text{ GPa}$), the length of debonding after arrest depends on the fiber break strength. The higher the strength at which the fiber breaks, the higher the strain energy that is released and higher the spring back of the broken fiber. This leads to higher debond lengths. The debond length vs fiber break strength curve shows a rapid increase in the debond length with break strength as shown in Fig. 11. In the presence of stable debonding, the ineffective length to reload the broken fiber is increased by the debond length as shown before in Fig. 7.

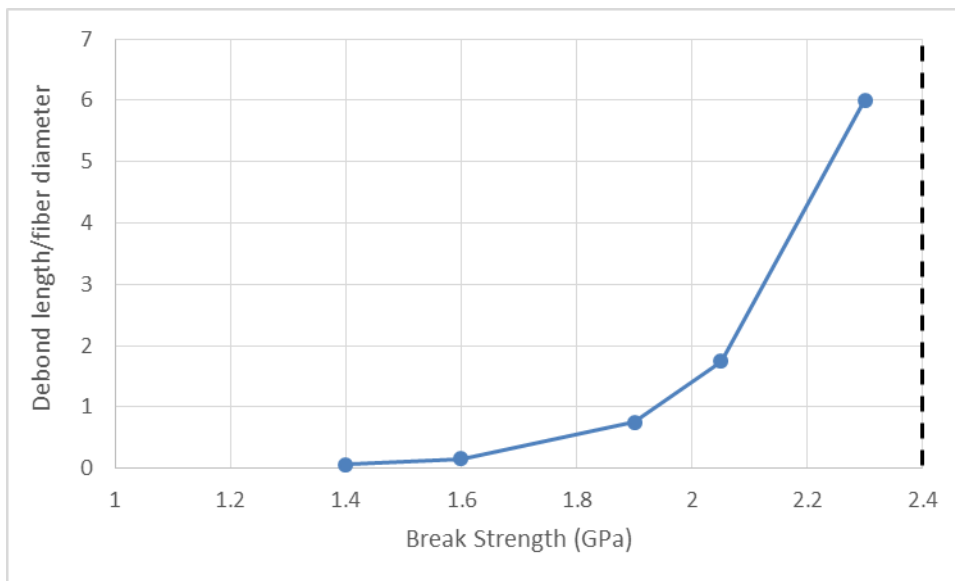


Fig 11: Normalized debond length (l_{deb}/d) vs break stress in Fiber 0 (σ_b)

Table II summarizes the SCFs and corresponding probabilities of failure (P_{fail}) that a fiber break at various break strengths will cause additional fiber breaks within the

zone of influence. Results are generated from the dynamic FE model and also the corresponding values obtained by solving the same problem using a quasi-static model with pre-broken fibers. In the static models, debonding does not initiate at break strengths below the critical splitting stress of 2.4 GPa. This makes the problem linear and hence, the SCF remains constant at around 1.25. Given the SCF and fiber strength distribution, the probability of failure increases in the adjacent fiber at $x/d=0$. If we take into account the dynamic effects, then there is a significant increase in the peak probability of additional fiber break in the adjacent fiber and due to the stress wave propagation, the location of this break can occur anywhere within the zone-of-influence. The slight reduction in peak SCF in the dynamic models with increase in fiber break strength (σ_b) is because of the energy dissipated through the interfacial debonding of the broken fiber. Table II also quantifies the size of the influence zone which is 5-6 times larger in area than the quasi-static result for fiber break strengths less than stability threshold.

The increase in the peak probability of failure due to the consideration of the dynamic effects of the fiber break may explain the discrepancy between the FE modeling results and experimental results reported in ¹⁷. The FE model used in ¹⁷ did not account for these dynamic effects and hence the model over-predicted the strain to failure in the composite as opposed to what was observed experimentally. The increased probability of failure in the neighboring fiber (Fiber 1) due to the dynamic stress wave propagation can also explain the formation of large clusters observed during a single strain increment in the experiment as opposed to the more gradual development of clusters as predicted by their FE model which assumed that the fiber break is a quasi-static process. Experimentally, 30% of all clusters observed were non-co-planar clusters (where adjacent fiber breaks are separated by an axial distance larger than a fiber radius). These clusters were formed within a single applied strain increment and did not grow further in size with additional applied strain. Since the zone of influence is 5-6 times larger in the dynamic models, it is expected that the model will predict a higher number of fiber breaks within this zone during the same applied strain increment. The clusters could thus be spread over a larger volume that is not limited by the ineffective length of the broken fiber. But at the same time, since the dynamic SCFs are significantly higher than the corresponding static SCFs in the neighboring fibers at the plane of the break, consideration of these dynamic effects could lead to the model predicting a higher percentage of co-planar breaks as well. The stochastics of strength distribution need to be incorporated in the model to better understand the interaction between these two effects and this will be the focus of our future work.

TABLE II. Increased probability of failure in Fiber 1 at different fiber break strengths in Fiber 0 (Comparison between Quasi-static and dynamic solutions)

Break stress (GPa)	Pfail before break	Static model SCF	Dynamic model Peak SCF	Pfail-Static	Pfail-Dynamic	Influence zone size ratio (Dynamic/Static)
1.4	1%	1.23	1.42	3%	6%	6.09
1.6	2%	1.24	1.42	5%	9%	5.21
1.9	4%	1.25	1.38	11%	17%	5.36
2.05	6%	1.25	1.38	16%	24%	5.33
2.3	10%	1.25	1.37	25%	35%	5.31
2.7	20%	1.13	1.30	31%	51%	Unstable debonding

Conclusions

The FE model presented in this paper enables us to visualize the dynamic progression of events after a brittle fiber fracture. The model has been validated using the analytical dynamic shear lag solution previously reported in literature^{6,20}. The dynamic SCF peaks propagate along the length of the neighboring fiber as a tensile stress wave which decays with distance from the plane of the fiber break. The compressive stress wave that is released in the broken fiber leads to dynamic interfacial debonding. The debond growth is stable up to a critical break strength which can be estimated using an energy balance criterion. Beyond this critical break strength, debonding propagates in an unstable manner along the entire length of the fiber given that interfacial debonding is the only energy dissipation mechanism considered in the present work. This unstable debonding cannot be predicted using quasi-static micromechanical models. Inclusion of other dissipation mechanisms such as matrix plasticity and friction between the debonded fiber and matrix into the stability criterion would increase the critical break strength at which unstable interface debonding would occur. These effects will be included in our future work. There is not only an increase in the peak failure probability of additional fiber breaks due to the consideration of dynamic stress concentrations, but there is also a significant increase in the size of the zone-of-influence of a fiber break. Since the stress waves in the fibers travel at the sound speed in S2-glass (6.06 km/s), the time-scales associated with the dynamic mechanisms reported in this paper are of the order of 10s of nanoseconds which is beyond the temporal resolution of current advanced high-speed

sensing capabilities ²¹ and hence cannot be visualized in real time. The results presented in this paper give us insights into key micromechanical failure mechanisms such as the propagation of dynamic stress concentrations as tensile stress waves over large distances in the neighboring fiber, and dynamic debond propagation in the interface surrounding the broken fiber. These mechanisms qualitatively agree with the experimental observations of damage in unidirectional fiber-reinforced composites under axial tensile loading ^{17,30}.

Acknowledgments

Research was sponsored by the Army Research Laboratory and was accomplished under Cooperative Agreement Number W911NF-12-2-0022. The views and conclusions contained in this document are those of the authors and should not be interpreted as representing the official policies, either expressed or implied, of the Army Research Laboratory or the U.S. Government. The U.S. Government is authorized to reproduce and distribute reprints for Government purposes notwithstanding any copyright notation herein.

References

1. Mishnaevsky L, Brøndsted P. Micromechanical modeling of damage and fracture of unidirectional fiber reinforced composites: A review. *Comput Mater Sci* 2009; 44: 1351–1359.
2. Swolfs Y, Gorbatiikh L, Verpoest I. Fibre hybridisation in polymer composites: A review. *Compos Part A Appl Sci Manuf* 2014; 67: 181–200.
3. Zweben C, Rosen BW. A statistical theory of material strength with application to composite materials. *J Mech Phys Solids* 1970; 18: 189–206.
4. Harlow DG, Phoenix SL. Probability Distributions for the Strength of Fibrous Materials under Local Load Sharing I: Two-Level Failure and Edge Effects. *Adv Appl Probab* 1982; 14: 68–94.
5. Cox HL. The elasticity and strength of paper and other fibrous materials. *Br J Appl Phys* 1952; 3: 72–79.
6. Hedgepeth JM. Stress Concentrations in Filamentary structures. NASA Tech Note 1961; D-882
7. Hedgepeth JM, Dyke P Van. Local Stress Concentrations in Imperfect Filamentary Composite Materials. *J Compos Mater* 1967; 1: 294–309.
8. Beyerlein IJ, Phoenix SL. Stress concentrations around multiple fiber breaks in an elastic matrix with local yielding or debonding using quadratic influence superposition. *J Mech Phys Solids* 1996; 44: 1997–2036.
9. Landis CM, McMeeking RM. Stress concentrations in composites with interface sliding, matrix stiffness and uneven fiber spacing using shear lag theory. *Int J Solids Struct* 1999; 36: 4333–4361.
10. Landis CM, McMeeking RM. A shear-lag model for a broken fiber embedded in a composite with a ductile matrix. *Compos Sci Technol* 1999; 59: 447–457.
11. Beyerlein IJ, Landis CM. Shear-lag model for failure simulations of unidirectional fiber composites including matrix stiffness. *Mech Mater* 1999; 31: 331–350.
12. Okabe T, Takeda N, Kamoshida Y, et al. A 3D shear-lag model considering micro-damage and statistical strength prediction of unidirectional fiber-reinforced composites. *Compos Sci Technol* 2001; 61: 1773–1787.
13. Nedele MR, Wisnom MR. Three-dimensional finite element analysis of the stress concentration at a single fibre break. *Compos Sci Technol* 1994; 51: 517–524.
14. Nedele MR, Wisnom MR. Stress concentration factors around a broken fibre in a unidirectional carbon fibre-reinforced epoxy. *Composites* 1994; 25: 549–557.
15. Goda K, Miwa Y, Kodama H. Effect of IFSS on tensile strength of unidirectional fiber composites using 3D-FEM simulation. *Adv Compos Mater* 2003; 12: 73–89.
16. van den Heuvel PWJ, Goutianos S, Young RJ, et al. Failure phenomena in fibre-reinforced composites. Part 6: A finite element study of stress concentrations in unidirectional carbon fibre-reinforced epoxy composites. *Compos Sci Technol*

2004; 64: 645–656.

17. Swolfs Y, Morton H, Scott AE, et al. Synchrotron radiation computed tomography for experimental validation of a tensile strength model for unidirectional fibre-reinforced composites. *Compos Part A Appl Sci Manuf* 2015; 77: 106–113.
18. Swolfs Y, McMeeking RM, Verpoest I, et al. Matrix cracks around fibre breaks and their effect on stress redistribution and failure development in unidirectional composites. *Compos Sci Technol* 2015; 108: 16–22.
19. Swolfs Y, McMeeking RM, Verpoest I, et al. The effect of fibre dispersion on initial failure strain and cluster development in unidirectional carbon/glass hybrid composites. *Compos Part A Appl Sci Manuf* 2015; 69: 279–287.
20. Xing Ji, Liu X-R, Chou T-W. Dynamic Stress Concentration Factors in Unidirectional Composites. *J Compos Mater* 1985; 19: 269–275.
21. Hudspeth M, Claus B, Parab N, et al. In Situ Visual Observation of Fracture Processes in Several High-Performance Fibers. *J Dyn Behav Mater* 2015; 1: 55–64.
22. Hartman D, Greenwood ME, Miller DM. High strength glass fibers. AGY Tech Pap 1996.
23. Sockalingam S, Dey M, Gillespie JW, et al. Composites : Part A Finite element analysis of the microdroplet test method using cohesive zone model of the fiber / matrix interface. *Compos Part A Appl Sci Manuf* 2014; 56: 239–247.
24. Song B, Chen W, Weerasooriya T. Quasi-Static and Dynamic Compressive Behaviors of a S-2 Glass/SC15 Composite. *J Compos Mater* 2003; 37: 1723–1743.
25. Weibull W. A Statistical Distribution Function of Wide Applicability. *J Appl Mech* 1951; 18: 293–297.
26. Gurvich MR, DiBenedetto a. T, Ranade S V. A New Statistical Distribution for Characterizing the Random Strength of Brittle Materials. *J Mater Sci* 1997; 32: 2559–2564.
27. Swolfs Y, Gorbatiikh L, Romanov V, et al. Stress concentrations in an impregnated fibre bundle with random fibre packing. *Compos Sci Technol* 2013; 74: 113–120.
28. Lucas JP, Moody NR, Robinson SL, et al. Determining fracture toughness of vitreous silica glass. *Scr Metall Mater* 1995; 32: 743–748.
29. Ochiai S, Schulte K, Peters PWM. Strain concentration factors for fibers and matrix in unidirectional composites. *Compos Sci Technol* 1991; 41: 237–256.
30. Shokrieh MM, Omidi MJ. Tension behavior of unidirectional glass/epoxy composites under different strain rates. *Compos Struct* 2009; 88: 595–601.